Egyptian Journal of Chemistry

Green Synthesis of Zinc oxide Nanocomposite Using Fusarium oxysporum and Evaluation of the Anticancer Effect on Hepatocellular Carcinoma

Doaa S. R. Khafaga [a,b,]*, Eid,M.M. [c], Mohamed Diaa Abd El-Maksoud [d], Mie afify [d], Mona H. Mohamed [e],

Abdel Razik H. Farrag [f], Rana A. A. Nagy [a], Heba K.A. Elhakim [a]

[a] *Biochemistry Division, Faculty of Science, Cairo University, Giza 12613, Egypt*
[b] *Faculty of Medicine, Galala University, Suez 43511, Egypt*
[c] *Spectroscopy Department, National Research Centre, Dokki, Giza 12622, Egypt*
[d] *Department of Biochemistry, Genetic Engineering and Biotechnology Research Division, National Research Centre, Dokki, Giza 12622, Egypt*
[e] *Department of Chemistry, Faculty of Science, Cairo University, Giza 12613, Egypt*
[f] *Professor of Histology and Histochemistry, Pathology Department, Medical Research Division, National Research Centre, Dokki, Giza 12622, Egypt*

Abstract

Nanoparticles can be synthesized by chemical, physical and biological system methods. In this work, Superparamagnetic Iron Oxide@Silver nanoparticles (SPION@Ag NPs) were modified by zinc oxide nanoparticles (ZnO NPs). SPION@Ag core shell NPs were synthesized by the biological method using Fusarium oxysporum fungus and coated with ZnO NPs. This method is eco-friendly and low cost. Characterization techniques such as UV, FTIR, HR-TEM, HR-SEM, XRD and zeta potential were used. The most common type of liver cancer is hepatocellular carcinoma (HCC). Hepatocellular carcinoma was induced by a single dose of diethyl nitrosamine (DEN) 60 mg/Kg b.wt. and was followed after two days by carbon tetra chloride (CCl_4) diluted with paraffin oil (50% v/v, 2 ml/Kg b.wt.) twice a week for one month. A histopathological examination was done after sacrifying. Clear changes were shown in the comparison between the HCC group treated with ZnO@SPION@Ag nanocomposite and the positive control group. Liver function tests showed a highly significant decrease after using the nanocomposite for HCC treatment. Our study aim is to evaluate the therapeutic anticancer effect of ZnO@SPION@Ag nanocomposite on hepatocellular carcinoma in male albino rats, which was synthesized by a new method called green chemistry or green synthesis.

1. Introduction

Hepatocellular carcinoma (HCC) is the most common primary liver tumour in the world, as well as the fifth most common malignancy and the third leading cause of cancer related mortality [1]. The majority of HCC cases evolve in the form of long-term inflammatory processes (i.e., chronic hepatitis and cirrhosis), predominantly as a result of HBV and HCV viral infections [2]. Age, gender, and any form of cirrhosis, as well as alcohol and aflatoxins, are all risk factors

[2]. Engineered nanoparticles (NPs) are used to treat diseases in nanomedicine, an area of biomedical application of nanotechnology. Nanomedicine has the potential for early cancer diagnosis and treatment due to its innovative imaging and therapeutic capabilities [3]. In contrast to standard cancer treatments, it has the advantages of active or passive targeting, high solubility, bioavailability, biocompatibility and multifunctionality [4]. ZnO nanoparticles less than 100 nm in size can be made in several forms, including solid, liquid (chemical) and gaseous. ZnO NPs were prepared by different chemical methods

_____

[5]. Due to their excellent physicochemical properties, protection and biodegradability [6]. ZnO NPs have therapeutic activity [7, 8]. It is now clear that ZnO NPs have a cytotoxic effect on tumour cells while causing minimal damage to healthy cells [9]. Superparamagnetic Iron Oxides (SPIONs) are particles formed by small crystals of iron oxide (commonly called magnetite Fe_3O_4 or maghemite Fe_2O_3) which may be surface modified to gain colloidal stability in aqueous media [10]. Several important criteria have to be considered for the SPION based drug delivery system to be effective. The coating/carrier should provide the delivery system with suitable hydrophilicity, so it can be easily dispersed in aqueous media. It should also provide functional groups which can be further modified to control the drug release or to bind targeting units [11]. Silver nanoparticles based nanosystems were evaluated as suitable carriers of various therapeutic molecules, including anti-inflammatory [12,13], antioxidant [14], antimicrobial [15, 16] and anticancer [17, 18] substances. Core–shell nanoparticles have received a lot of attention, especially as multimodal for medical applications [19–22]. Several methods have been employed for the synthesis of nanoparticles. Among them, clean and eco-friendly green chemistry is an interesting route that has emerged recently [23, 24]. Fungi are among the organisms that have been employed for down-up synthesis [24–26]. The fungus Fusarium oxysporum can reduce aqueous silver ions extracellularly to generate silver nanoparticles (Ag NPs) [27]. In the present study, we aim to evaluate the anticancer effect of ZnO@SPION@Ag nanocomposite on hepatocellular carcinoma in male albino rats.

2. Materials and methods

2.1. Chemicals

Iron (III) nitrate ($Fe(No_3)_3$) 99.0-101.0 %, ammonium iron (II) sulfate hexahydrate (($NH_4)_2Fe(SO_4)_2.6H_2O$) 99.0-101.5 % and Silver nitrate ($AgNO_3$) 99.8-100.5 % were purchased and used as received from Merck (Germany). Sodium hydroxide (NaOH) and zinc acetate (($CH_3CO_2)_2Zn$) 99.99 % were purchased from sigma Aldrich. Carbon tetrachloride (CCl_4) was purchased from Al-Gomhorya Company Pharmaceutical, Cairo, Egypt. Diethyl Nitrosamine (DEN) was purchased from Gene Tech Company.

2.2. Biological synthesis of SPION@Ag core shell nanoparticles

The synthesis method depends on the deposition of Ag atoms onto the seeds of the SPION NPs via the control reduction of Ag precursor in a growth solution containing iron oxide nanoparticles [28]. Fusarium oxysporum fungi were obtained from the microbiology department of National Research Centre, Dokki, Giza, Egypt. The fungal mycelia were carefully separated from the filtrate under antiseptic conditions. The seed of Ag NPs was prepared as follows: 0.1027 g $AgNO_3$ was added to fungus mycelia in 300 ml of distal water with vigorous shaking at 37°C for 1 hour, and the pH was adjusted to 9. The solution of SPION NPs seed has been prepared by adding 0.4174 g $Fe(NO_3)_3$ and 0.3002 g $(NH_4)_2Fe(SO_4)_2.6H_2O$ in 50 ml sterile distilled water under vigorous shaking at 70°C for 1 hour, and the pH was adjusted to 12. The two solutions were mixed under shaking at 37°C for 72 hours. The nanoparticles were centrifuged and washed. The formation of the core–shell has been examined by UV/Visible and FTIR spectroscopy. The functionalization of chitosan active groups on the surface of the nanocomposite is spontaneous in the reaction mechanism due to the presence of chitin (a deacetylated form of chitosan in the cell wall of the fungus), i.e. we did not add chitosan to the reaction.

2.3. Synthesis of ZnO nanoparticles (ZnO NPs)

5 g of zinc acetate was dissolved in 100 ml distal water then heated for 40-50°C and at the same time, 10 M sodium hydroxide was prepared. Sodium hydroxide was added drop by drop to the wall of the flask contain zinc acetate for 30-45 min. After precipitation occurs, wash precipitate twice and dry at 50°C, then calcination at 400°C based on Ghorbani et al. method [29] with some modification.

2.4. Synthesis of ZnO-coated Superparamagnetic Iron Oxide@Silver (ZnO@SPION@Ag) nanocomposite

An equal amount of two nano-powders (SPION@Ag NPs core shell + ZnO NPs) were added to each other and were ground by mortar then dissolved in 25 ml distal water then sonication for 45 sec. Finally, the obtained nanocomposites were dried overnight at 40°C now the nanocomposite is ready to use.

_____

_____

2.5. ZnO@SPION@Ag nanocomposite characterization

UV\Visible absorption spectrophotometer (JASCO V-630) with a resolution of 0.2 nm is used for the detection of the best conditions for the biosynthesis of core–shell nanoparticles. Liquid samples were diluted with distilled water at a 1:4 ratio and scanned in the range of 200 to 800 nm. Fourier transform infrared spectroscopy analysis was performed to study the molecular structure of the nanocomposite and the capping layer that decorates the nanoparticles to understand the mechanism of preparation. The transmission spectrum was acquired for the MID-Far range using diamond cells. The spectra were recorded using a Vertex 70 Bruker Transform Infrared spectrophotometer at a resolution of 1 cm^{-1} in the range between 4000 and 400 cm^{-1}. The morphology and structure of samples were determined using HRTEM (JEM-2100HR, Japan) at 200 KeV. XRD analyses were recorded on a Bruker D-8 powder X-ray diffractometer using Cu Kα radiation (λ=0.15418 nm) over a 2θ range of 20°-90° with a step of 0.02. Zeta potential was determined by the dynamic light scattering (DLS) technique using a PSS-NICOMP 380-ZLS, USA.

2.6. Induction of the hepatocellular carcinoma

HCC was induced by a single dose of DEN at 60 mg/Kg b.wt., followed by CCl$_4$ diluted with paraffin oil (50% v/v, 2 ml/Kg b.wt.) twice a week for one month.

2.7. Experimental animal

24 male albino rats (76-130 g) were obtained from the National Research Centre (NRC) Dokki, Giza, Egypt. The animals were housed in suitable plastic cages (8 rats/cage) with stainless steel wire lids. Rats were kept in standard laboratory conditions (12-hour light/dark cycle), fed a standard diet, and given water. All animal procedures were directed in agreement with the recommendation criteria of experimental animal care and the current protocol was accepted (Approval no. CU/I/F/100/17). Animals were categorized into 3 groups, with 8 rats in each group. **Group (I):** Negative control group, **Group (II):** Positive control group; rats were induced with HCC, **Group (III):** HCC rats were treated by ZnO@SPION@Ag nanocomposite (10 mg/Kg b.wt.) daily for 15 days.

2.8. Histopathological examination

Specimens were washed in tap water, dehydrated in ethanol in ascending grades, cleared in xylene, and embedded in paraffin wax (melting point 56-60ºC). Sections of 6 μm thickness were prepared and stained with haematoxylin and eosin [30]. In this method, the paraffin sections were stained with harris haematoxylin for 5 minutes. Sections were washed in running water for blueing and then stained in 1 % watery eosin for 2 minutes, washed in water, dehydrated, cleared and mounted in canada balsam. The cytoplasm was stained in shades of pink to red, and the nuclei gave a blue color.

2.9. Biochemical analysis

Routine liver function testes transaminases were assayed according to Henry RJ et al. [31] and alpha feto protein (AFP) was determined by enzyme linked immunosorbent (ELISA) according to Bates SE [32] which estimated agree to construction protocol of colorimetric kits (Spectrum kits) and antioxidant parameters assay in liver tissue were investigated as malonaldhyde (MDA) [33] and superoxide dismutase (SOD) [34] which estimated agree to construction protocol of colorimetric kits (Biodiagnostic kits).

3. Results and Discussion

### 3.1. Physico-chemical characterization of ZnO@SPION@Ag nanocomposite

UV–Vis absorption spectra of ZnO NPs and ZnO@SPION@Ag nanocomposite. The excitonic transfer of electrons from the valence band to the conduction band of ZnO NPs is connected with the significant absorption peak in the UV region at wavelengths of 300–400 nm. In the UV range, ZnO@SPION@Ag nanohybrid has reduced absorbance intensity. The UV-range emission, also known as radiative recombination occurs in ZnO materials. The different surface plasmon resonance (SPR) effects of nanoscale Ag metals cause variances in UV light emission intensity. The high-density electrons of noble metal nanoparticles form an electron cloud and oscillate when light with a wavelength greater than the particle size is absorbed. When noble metal nanoparticles are mixed with ZnO, electrons collect at the metal ZnO interface, causing the ZnO side's band to bend downward, allowing for facile electron transfer from the Ag nanoparticles to the ZnO side. For ZnO@SPION@Ag NP the energy band gap of ZnO has decreased from 3.4 to 2.6 ev Fig.1.

_____
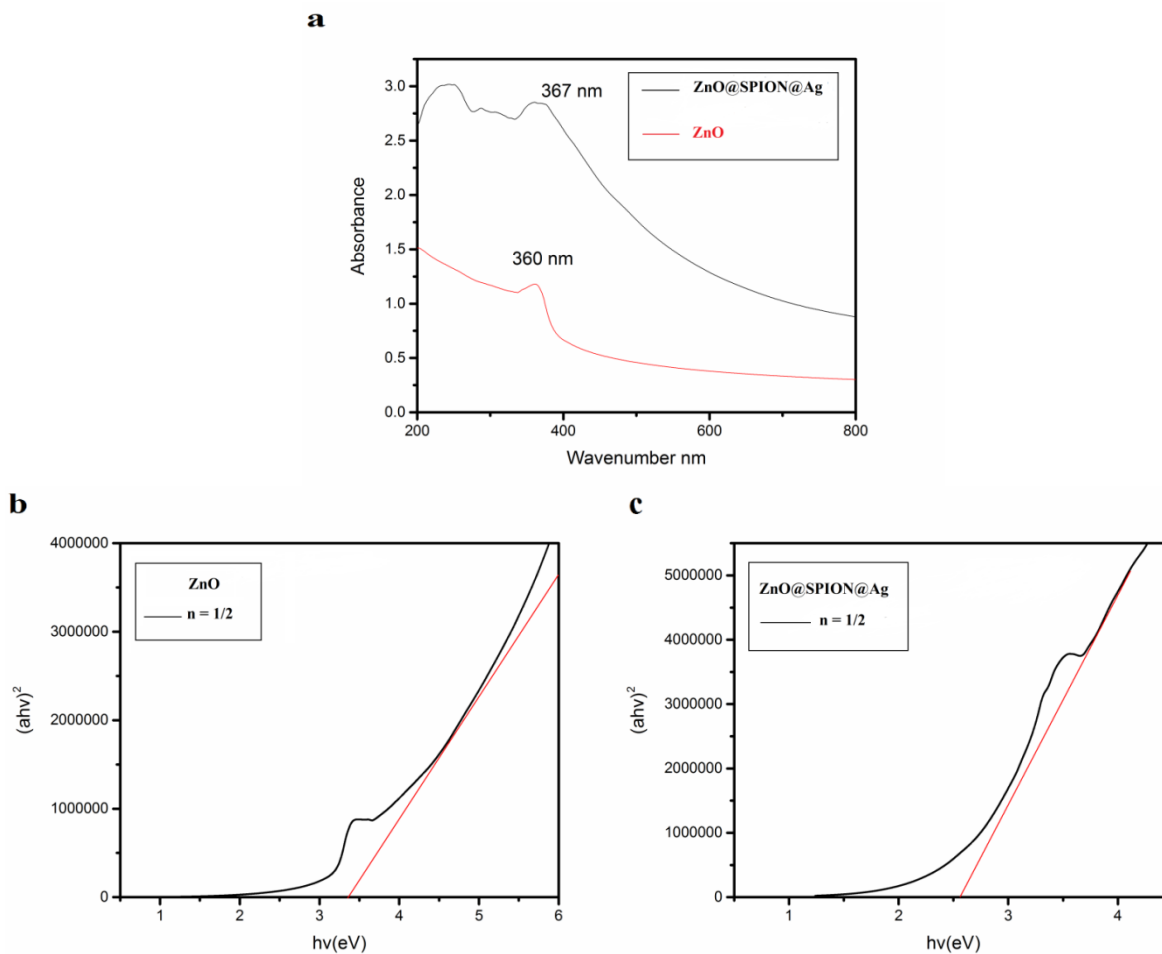
Fig.1. (a) UV-Vis. of ZnO and ZnO@SPION@Ag NPs, (b and c) ZnO NPs and ZnO@SPION@Ag NPs energy band gap for n=1/2

The structure of the nanocomposite was confirmed using fourier transform IR Fig.2. The production of ZnO@SPION@Ag NP has been validated by a decrease in the intensity of the ZnO band and a blue shift to 432 cm^{-1} which confirms the production of ZnO@SPION@Ag NP.
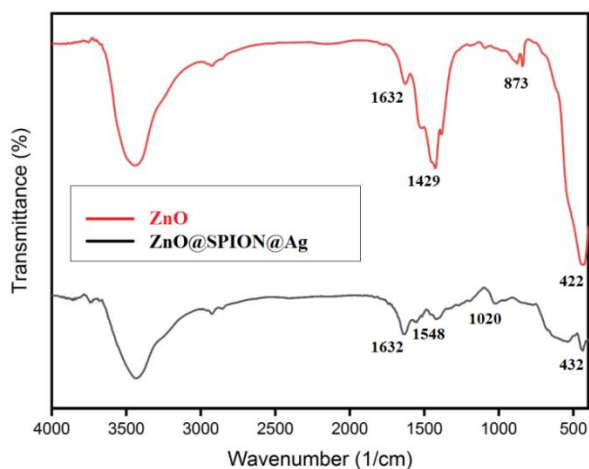
Fig.2. The Molecular structure confirmation of the nanocomposite, FTIR transmission spectrum of ZnO NPs and ZnO@SPION@Ag NPs

The morphology of ZnO NPs is shown in the HR-TEM images in Fig.3 (a). The high-density dumbbell-like ZnO NPs with a diameter ranging from 10-30 nm. The high resolution TEM (HRTEM) image in Fig.3 (a) displays the clear lattice fringes of 2.38 Å, which correspond to the d-spacing of the (101) crystal planes of hexagonal ZnO in consistence with the XRD results. The selected area electron diffraction (SAED) pattern shown in Fig.3 (b) confirms the polycrystalline structure of the ZnO NPs and the ZnO@SPION@Ag nanocomposite with diameter of 50-100 nm Fig.3 (e). HR-SEM is shown in Fig.3 (c and f) for ZnO and ZnO@SPION@Ag NPs.
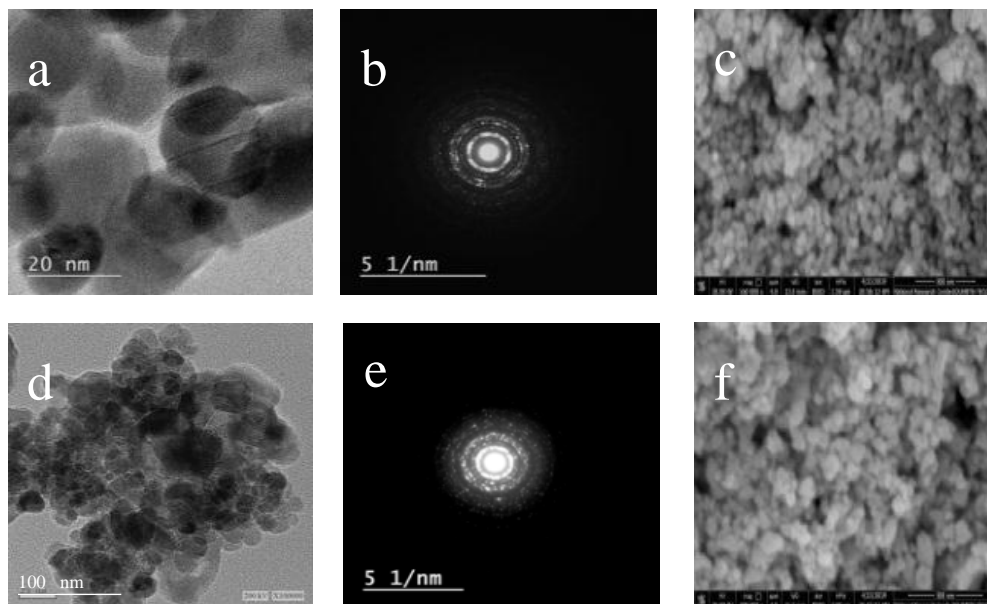
Fig.3. HRTEM of ZnO NPs and ZnO@SPION@Ag NPs (a and d), SAED pattern of ZnO and ZnO@SPION@Ag (b and e) and HRSEM of ZnO NPs and ZnO@SPION@Ag NPs (c and f)

The XRD pattern of biosynthesized ZnO NPs shown in Fig.4 (a) confirms the production of the nanocrystalline phase with well-defined relatively broad peaks of high intensity. By using the Joint Committee on Powder Diffraction Standards (JCPDS) card no. 36–1451; the acquired peaks are indexed inside the hexagonal ZnO wurtzite-type structure.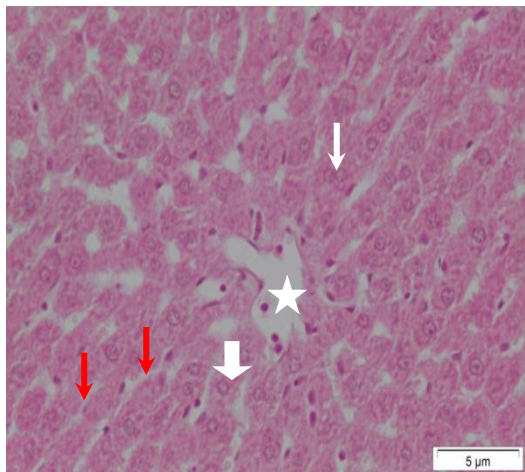 The XRD pattern of biosynthesized ZnO NPs in Fig.4 (a) confirms well-defined, relatively broad peaks with high intensity, confirming the development of the ZnO@SPION@Ag. In Fig.4 (b), the appearance of the 100 planes of ZnO and the 200 planes of SPION@Ag confirms the development of the ZnO@SPION@Ag. The ZnO@SPION@Ag NP has an average zeta potential of -38 mV.
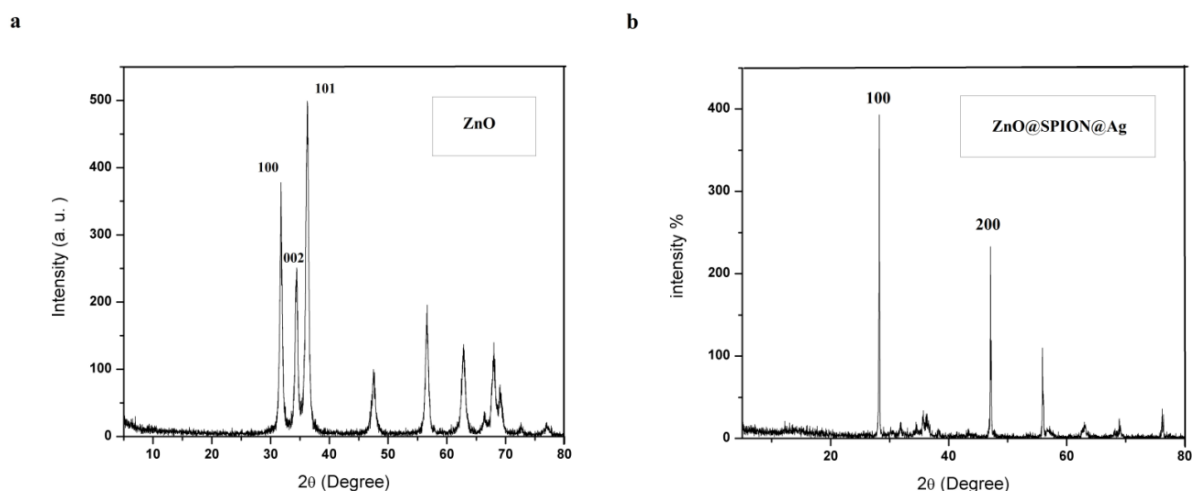
**Fig.4.** XRD of ZnO NPs (a) and ZnO@SPION@Ag NPs (b)

_____

3.2. Histopathological examination and biochemical analysis

Histopathological examination of liver sections from the control group showed normal hepatocytes radiating from the central vein. The hepatocytes show vesicular nuclei, some of which are

binucleated and sinusoids separate the strands of liver cells Fig.5. In addition, normal portal tract with its structures; brances of portal wein, hepatic artery and bile duct Fig.6.
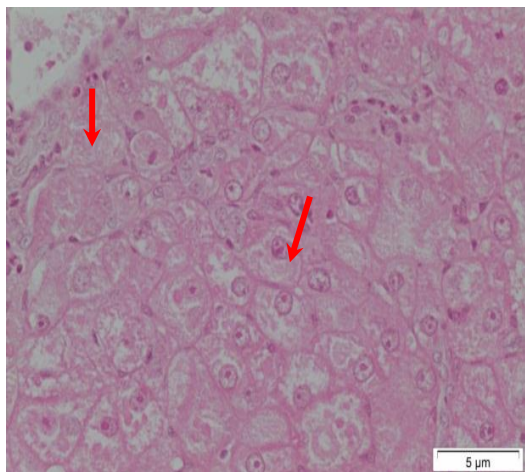

Fig.5. A micrograph of a section from the liver of the normal control group showing normal hepatocytes (arrows) radiating from the central vein (asterisk). The hepatocytes showing vesicular nuclei (arrowhead) some of the hepatocytes are binucleated and separated with sinusoids (red arrow) **(H&E stain, Scale bar: 5 µm)**
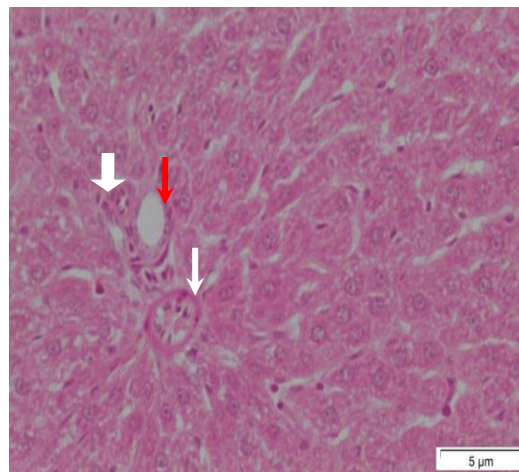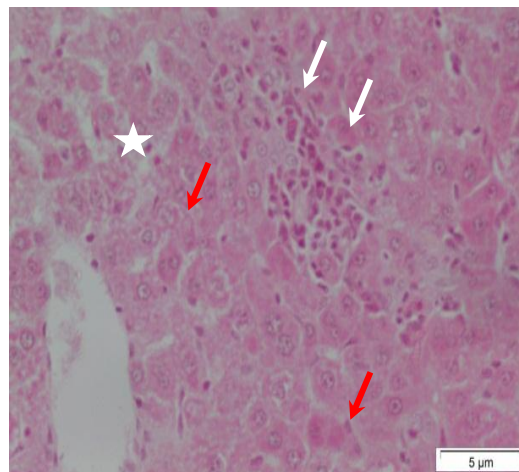

Fig.6. A micrograph from the liver of the normal control group showing normal portal tract with its structures; branches of the portal vein (arrow), hepatic artery (arrowhead) and bile duct (red arrow) **(H&E stain, Scale bar: 5 µm)**

HCC was induced by DEN at a dose of 60 mg/kg b.wt. and after 2 days given CCl$_4$ at a dose of 2 ml/kg b.wt. twice a week for 1 month showed a pale pink appearance of the cytoplasm of hepatocytes that
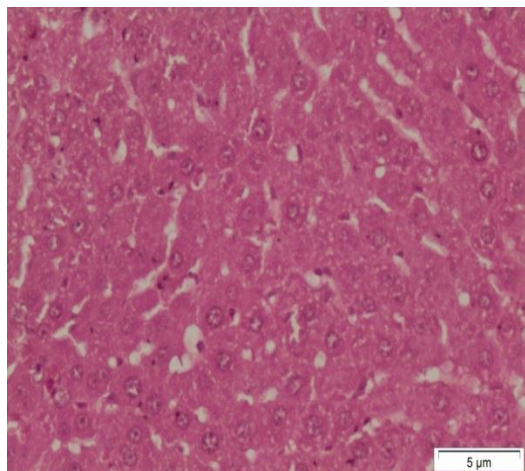
appeared as ground-glass hepatocytes Fig.7. Acute inflammation, pale stained hepatocytes, focal necrosis, and dead cells stained bright pink or eosinophilia are present in Fig. 8.

Fig.7. A micrograph from the liver of rat administered DEN at a dose of 60 mg/kg b.wt. and after 2 days given CCl$_4$ at a dose of 2 ml/kg b.wt. twice a week for 1 month showing the cytoplasm of hepatocytes may assume an even pale pink appearance such ground-glass hepatocytes (arrows) **(H&E stain, Scale bar: 5 µm)**

Fig.8. A micrograph from the liver of rat administered DEN at a dose of 60 mg/kg b.wt. and after 2 days given CCl$_4$ at a dose of 2 ml/kg b.wt. twice a week for 1 month showing acute inflammation in the hepatocytes (arrows) many of the hepatocytes are pale stained and a few exhibit necrosis (asterisk). The dead cells stain a bright pink eosinophilia (red arrows) **(H&E stain, Scale bar: 5 µm)**
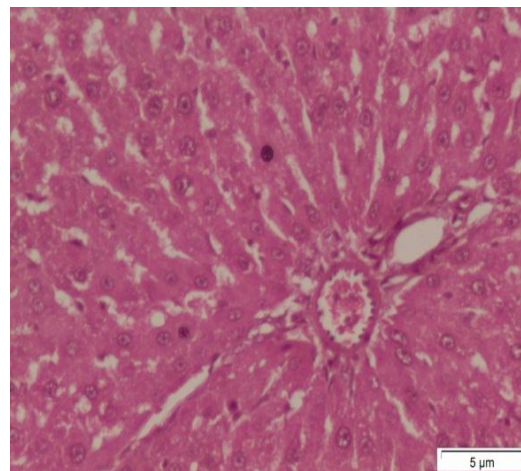
_____

A section of the liver from rats given DEN at a dose of 60 mg/kg b.wt. and then given CCl$_4$ at a dose of 2 ml/kg b.wt. twice a week for 1 month, then injected with ZnO@SPION@Ag core-shell for 15 times revealed that both the hepatic lobules Fig.9 and portal tracts appeared more or less normal Fig.10.

Fig.9. A micrograph from the liver of rat administered DEN at a dose of 60 mg/kg b.wt. and after 2 days given CCl$_4$ at a dose of 2 ml/kg b.wt. twice a week for 1 month then injected with ZnO@SPION@Ag core–shell for 15 times the hepatic lobule appeared more or less like normal **(H&E stain, Scale bar: 5 μm)**

Fig.10. A micrograph from the liver of rat administered DEN at a dose of 60 mg/kg b.wt. and after 2 days given CCl$_4$ at a dose of 2 ml/kg b.wt. twice a week for 1 month then injected with ZnO@SPION@Ag core–shell for 15 times showing the portal tract appeared more or less like normal **(H&E stain, Scale bar: 5 μm)**

Table 1 depicts the therapeutic potential of ZnO@SPION@Ag nanocomposite on serum activity of liver enzymes in the HCC rat model. In comparison with the negative control group, there was a highly significant increase at P-value < 0.01 in serum ALT, AST, and AFP activity of the positive control group, while the treated HCC group elucidated a highly significant decrease in serum ALT, AST and AFP activity as compared with the positive control group.

Table 1 Each value represents the mean ± SD. (a) significant compared with group I (Negative control), (b) significant compared with group II (Positive control)

		G I	G II	G III
ALT (U/l)	Mean ± SD	49.75 ± 5.258	93.625 ± 11.413 [a]	67.25 ± 5.23 [a,b]
AST (U/l)	Mean ± SD	256 ± 39.155	409.5 ± 63.628 [a]	371.375 ± 56.237 [a]
AFP (ng/ml)	Mean ± SD	0.188 ± 0.083	10.625 ± 1.302 [a]	0.5 ± 0.2 [b]

Hepatocellular carcinoma is a common malignant tumour located in hepatic or hepatobiliary cells and presents a high mortality rate. The incidence of HCC morbidity is approximately 850,000 new cases per year [35]. Hepatic injury caused by DEN is typically characterized by changes in liver metabolism that result in distinct changes in serum enzyme activities [36]. Intracellular enzymes like transaminases are good indicators of liver function and their elevated levels indicate liver damage. Aminotransferases (AST and ALT) are reliable liver marker enzymes and the first enzymes used in diagnostic enzymology when liver damage occurs [37]. Because of their intracellular position in the cytosol, toxicity affecting the liver results in their spillage into serum where their concentration increases due to a breakdown in cell membrane architecture [38]. According to Tayel A et al., 2014 [39] and Al-Rejaie, S. S. et al., 2008 [40] there was a huge turnover of hepatocytes and a large rise in serum has been shown to be Activities of ALT, AST in DEN Induced population of hepatocellular carcinoma as compared with the negative control group. In the untreated HCC control group, serum levels of AFP were significantly increased relative to their values in normal rats [41]. Our study results agree with previous studies and ZnO@SPION@Ag nanocomposite significantly decreases the enzymes activity in the HCC treated group when compared with the positive control group Fig.11.
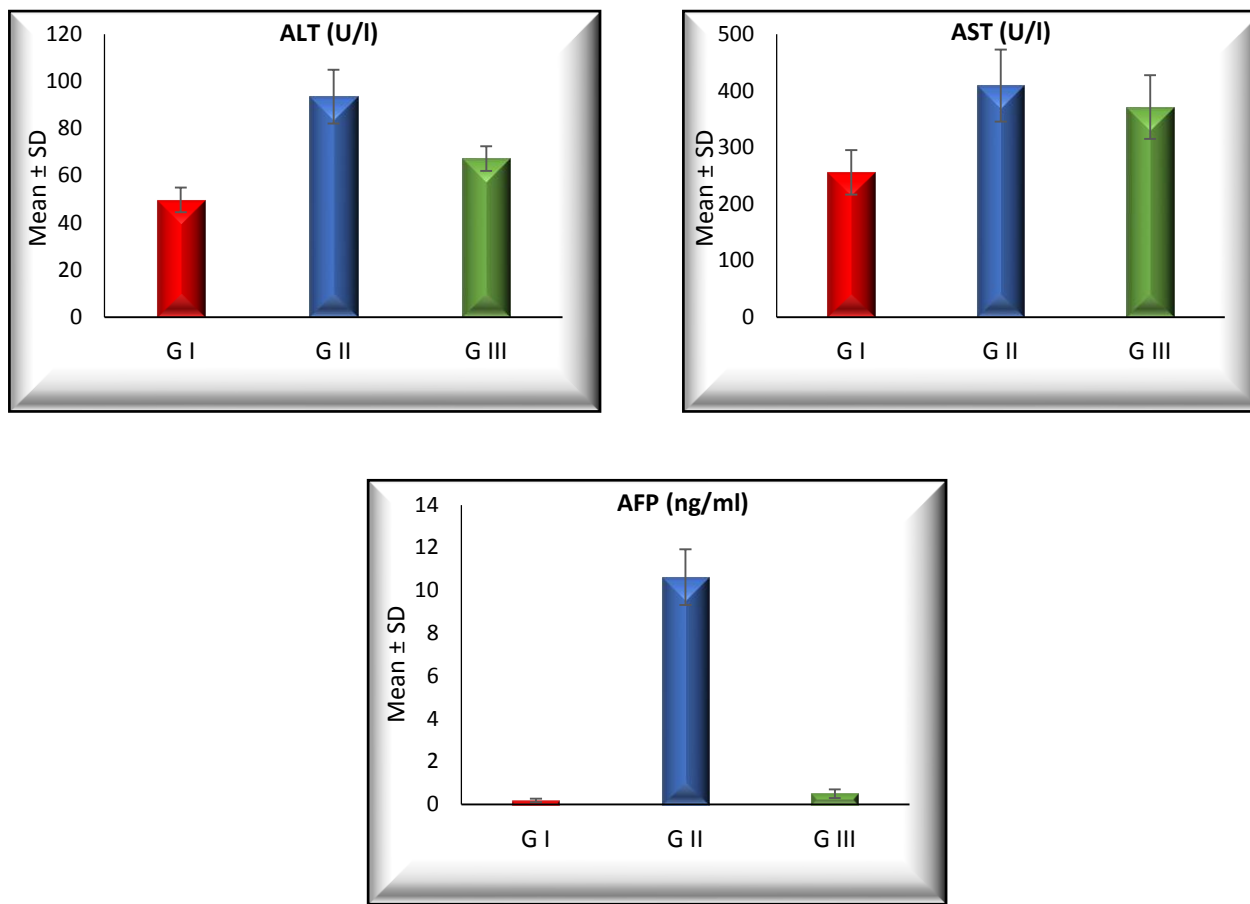
Fig.11. Mean ± SD of liver function tests

The data illustrated in table 2 shows the therapeutic potential of ZnO@SPION@Ag nanocomposite on liver tissue antioxidants activity in the HCC rat model. In comparison between the studied groups, there was a highly significant at P-value 0.001.

Table 2 Each value represents the mean ± SD. (a) significant compared with group I (Negative control), (b) significant compared with group II (Positive control)

		G I	G II	G III
MDA nmol/g.tissue	Mean ± SD	11 ± 3.665	23.75 ± 8.259 [a]	16.125 ± 6.446
SOD U/gm tissue	Mean ± SD	361.5 ± 75.495	320.875 ± 29.997	431.375 ± 69.455 [b]

Lipid peroxides, calculated as MDA, are widely used as one of the most effective oxidative stress indices to assess oxidative damage in patients with liver injury [42–44]. Increased levels of MDA contribute to the pathogenesis of several metabolic diseases including cancer [45]. Our study revealed a highly significant increase in MDA level at P–value < 0.001 when comparing between the positive control group and the negative control group, and when using

ZnO@SPION@Ag nanocomposite for HCC treatment, the level of MDA highly significant decrease at P-value 0.004 but SOD level non-significant decrease at P-value 0.728 in comparing between the positive control group and the negative control group and when using ZnO@SPION@Ag nanocomposite for HCC treatment the level of SOD significant increase at P-value 0.015 Fig.12. This is supported by a recent DEN/CCl₄ study by Zhang et

al. 2016 [46], who found that DEN can induce HCC by interacting with strategic macromolecules including antioxidant enzymes, DNA, lipids and DNA repairing system enzymes. Furthermore, it is widely recognized that CCl_4 biotransformation by cytochrome P-450 results in the formation of trichloromethyl free radical (CCl_3^*) and trichloromethyl proxy free radical (CCl_3OO^*) as two

metabolites linked to ROS generation, lipid peroxidation and a decrease in SOD enzymatic activity [47–49]. Furthermore, the findings are consistent with those of Hussein & Khalifa and Kadasa et al. [50, 51], who found a substantial decrease in antioxidant enzyme activities in DEN induced rats as compared to control.
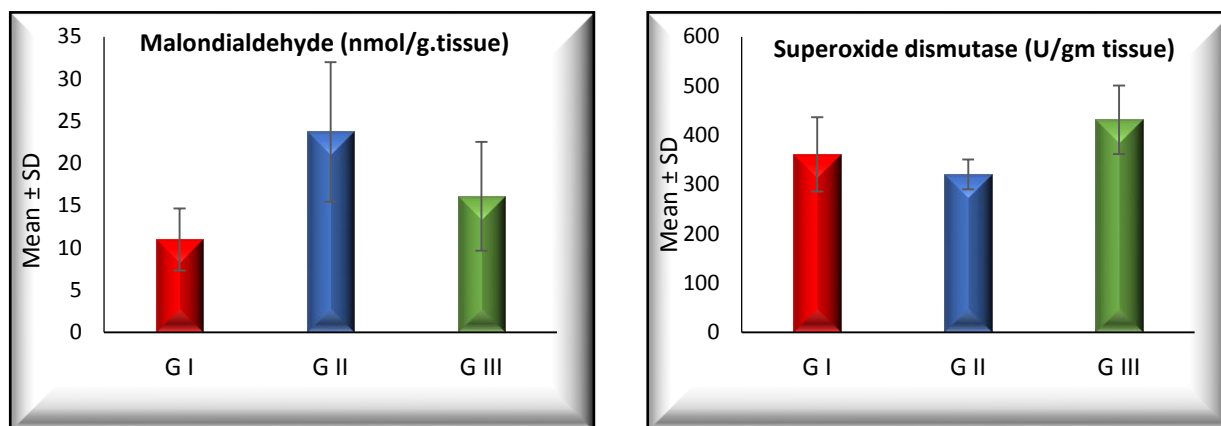

Fig.12. Mean ± SD of antioxidants activity

4.   Conclusion

Nanoparticles synthesized by the biological system have low side effects on normal cells and SPION targeted the nanocomposite to the specific site of cancer, so ZnO@SPION@Ag nanocomposite can be used as anticancer for HCC according to histopathological changes that occurred after treatment.

5.   Conflicts of interest

There are no conflicts to declare

6.   Formatting of funding sources

No Fund

References

1. Sundaresan, S. & Rajapriya, P. *Translational Perspective in Hepatocellular Carcinoma. Translational Research in Cancer* (IntechOpen, 2020). doi:10.5772/intechopen.94769

2. Perisetti, A., Goyal, H., Yendala, R., Thandassery, R. B. & Giorgakis, E. Non-cirrhotic hepatocellular carcinoma in chronic viral hepatitis: Current insights and advancements. *World J Gastroenterol* **27**, 3466–3482 (2021)

3. Mitchell, M. J. *et al.* Engineering precision nanoparticles for drug delivery. *Nat Rev Drug Discov* **20**, 101–124 (2021)

4. McNeil, S. E. Nanoparticle therapeutics: a personal perspective. *WIREs Nanomedicine and Nanobiotechnology* **1**, 264–271 (2009)

5. Li, Y., Liao, C. & Tjong, S. C. Recent Advances in Zinc Oxide Nanostructures with Antimicrobial Activities. *Int J Mol Sci* **21**, 8836 (2020)

6. Zhou, J., Xu, N. S. & Wang, Z. L. Dissolving Behavior and Stability of ZnO Wires in Biofluids: A Study on Biodegradability and Biocompatibility of ZnO Nanostructures. *Advanced Materials* **18**, 2432–2435 (2006)

7. Jin, S.-E. & Jin, H.-E. Synthesis, Characterization, and Three-Dimensional Structure Generation of Zinc Oxide-Based Nanomedicine for Biomedical Applications. *Pharmaceutics* **11**, 575 (2019)

8. Hu, C. & Du, W. Zinc oxide nanoparticles (ZnO NPs) combined with cisplatin and gemcitabine inhibits tumor activity of NSCLC cells. *Aging (Albany NY)* **12**, 25767–25777 (2020)

_____

9. Rasmussen, J., Martinez, E., Louka, P. & Wingett, D. Zinc Oxide Nanoparticles for Selective Destruction of Tumor Cells and Potential for Drug Delivery Applications. *Expert opinion on drug delivery* **7**, 1063–77 (2010)

10. Samrot, A. V., Sahithya, C. S., Selvarani A, J., Purayil, S. K. & Ponnaiah, P. A review on synthesis, characterization and potential biological applications of superparamagnetic iron oxide nanoparticles. *Current Research in Green and Sustainable Chemistry* **4**, 100042 (2021)

11. Dulińska-Litewka, J. *et al.* Superparamagnetic Iron Oxide Nanoparticles—Current and Prospective Medical Applications. *Materials (Basel)* **12**, 617 (2019)

12. Barczikai, D., Kacsari, V., Domokos, J., Szabó, D. & Jedlovszky-Hajdu, A. Interaction of silver nanoparticle and commonly used anti-inflammatory drug within a poly(amino acid) derivative fibrous mesh. *Journal of Molecular Liquids* **322**, 114575 (2021)

13. Tyavambiza, C., Elbagory, A. M., Madiehe, A. M., Meyer, M. & Meyer, S. The Antimicrobial and Anti-Inflammatory Effects of Silver Nanoparticles Synthesised from Cotyledon orbiculata Aqueous Extract. *Nanomaterials (Basel)* **11**, 1343 (2021)

14. Bedlovičová, Z., Strapáč, I., Baláž, M. & Salayová, A. A Brief Overview on Antioxidant Activity Determination of Silver Nanoparticles. *Molecules* **25**, E3191 (2020)

15. Skóra, B. *et al.* Noncytotoxic silver nanoparticles as a new antimicrobial strategy. *Sci Rep* **11**, 1–13 (2021)

16. Enan, E. T., Ashour, A. A., Basha, S., Felemban, N. H. & El-Rab, S. M. F. G. Antimicrobial activity of biosynthesized silver nanoparticles, amoxicillin, and glass-ionomer cement against Streptococcus mutans and Staphylococcus aureus. *Nanotechnology* **32**, 215101 (2021)

17. Ahn, E.-Y. & Park, Y. Anticancer prospects of silver nanoparticles green-synthesized by plant extracts. *Mater Sci Eng C Mater Biol Appl* **116**, 111253 (2020)

18. Dilshad, E. *et al.* Synthesis of Functional Silver Nanoparticles and Microparticles with Modifiers and Evaluation of Their Antimicrobial, Anticancer, and Antioxidant Activity. *J Funct Biomater* **11**, E76 (2020)

19. Pillarisetti, S. *et al.* Multimodal Composite Iron Oxide Nanoparticles for Biomedical Applications. *Tissue Eng Regen Med* **16**, 451–465 (2019)

20. Ali Dheyab, M., Abdul Aziz, A., Jameel, M. S. & Moradi Khaniabadi, P. Recent Advances in Synthesis, Medical Applications and Challenges for Gold-Coated Iron Oxide: Comprehensive Study. *Nanomaterials (Basel)* **11**, 2147 (2021)

21. Srinivasan, S. Y., Paknikar, K. M., Gajbhiye, V. & Bodas, D. Magneto-Conducting Core/Shell Nanoparticles for Biomedical Applications. *ChemNanoMat* **4**, 151–164 (2018)

22. Stafford, S., Serrano Garcia, R. & Gun'ko, Y. K. Multimodal Magnetic-Plasmonic Nanoparticles for Biomedical Applications. *Applied Sciences* **8**, 97 (2018)

23. Proniewicz, E. *et al.* SERS activity and spectroscopic properties of Zn and ZnO nanostructures obtained by electrochemical and green chemistry methods for applications in biology and medicine. *Phys Chem Chem Phys* **22**, 28100–28114 (2020)

24. Bhardwaj, K. *et al.* Conifer-Derived Metallic Nanoparticles: Green Synthesis and Biological Applications. *Int J Mol Sci* **21**, E9028 (2020)

25. Alavi, M. & Nokhodchi, A. Synthesis and modification of bio-derived antibacterial Ag and ZnO nanoparticles by plants, fungi, and bacteria. *Drug Discov Today* **26**, 1953–1962 (2021)

26. Fahmy, S. A., Preis, E., Bakowsky, U. & Azzazy, H. M. E.-S. Platinum Nanoparticles: Green Synthesis and Biomedical Applications. *Molecules* **25**, E4981 (2020)

27. Rai, M. *et al.* Fusarium as a Novel Fungus for the Synthesis of Nanoparticles: Mechanism and Applications. *J Fungi (Basel)* **7**, 139 (2021)

28. Eid, M. M. *et al.* Preparation conditions effect on the physico-chemical properties of magnetic–plasmonic core–shell nanoparticles functionalized with chitosan: Green route. *Nano-Structures & Nano-Objects* **16**, 215–223 (2018)

29. Ghorbani, H., Mehr, F., Pazoki, H. & Rahmani, B. Synthesis of ZnO Nanoparticles by Precipitation Method. *Orient. J. Chem* **31**, 1219–1221 (2015)

30. Shawi, O. E. E., El-Rahman, S. S. A. & Hameed, M. A. E. Reishi Mushroom Attenuates Hepatic Inflammation and Fibrosis Induced by Irradiation Enhanced Carbon Tetrachloride in Rat Model. *Journal of Biosciences and Medicines* **3**, 24–38 (2015)

31. Essodolom, P. et al. Evaluation du statut nutritionnel et biologique d'un échantillon de personnes atteintes de glaucome à angle ouvert dans une population togolaise. International Journal of Biological and Chemical Sciences 8, 1535 (2015)

32. Zhao, H.-C., Xu, Q.-S., Shi, Y.-B. & Ma, X.-J. Clinical-radiological predictive model in differential diagnosis of small (≤ 20 mm) solitary pulmonary nodules. BMC Pulm Med 21, 281 (2021)

33. Ohkawa, H., Ohishi, N. & Yagi, K. Assay for lipid peroxides in animal tissues by thiobarbituric acid reaction. Anal Biochem 95, 351–358 (1979)

34. Medeiros, L. H. C. et al. Chondroitin sulfate from fish waste exhibits strong intracellular antioxidant potential. Braz J Med Biol Res 54, e10730 (2021)

_____

35. Ding, X.-X. *et al.* Precision medicine for hepatocellular carcinoma: driver mutations and targeted therapy. *Oncotarget* **8**, 55715–55730 (2017)

36. Whitby, L. G., Percy-Robb, I. W. & Smith, A. F. *Lecture notes on clinical chemistry.* (Blackwell Scientific Publications, 1984)

37. Lippert, M., Papadopoulos, N. & Javadpour, N. Role of lactate dehydrogenase isoenzymes in testicular cancer. *Urology* **18**, 50–53 (1981)

38. Canbek, M. *et al.* Effects of carvacrol on defects of ischemia-reperfusion in the rat liver. *Phytomedicine* **15**, 447–452 (2008)

39. Tayel, A. *et al.* Suramin inhibits hepatic tissue damage in hepatocellular carcinoma through deactivation of heparanase enzyme. *Eur J Pharmacol* **728**, 151–160 (2014)

40.Al-Rejaie, S. S. et al. Progression of diethylnitrosamine-induced hepatic carcinogenesis in carnitine-depleted rats. World J Gastroenterol 15, 1373–1380 (2009)

41. Hassan, H. F. H., Mansour, A. M., Abo-Youssef, A. M. H., Elsadek, B. E. M. & Messiha, B. A. S. Zinc oxide nanoparticles as a novel anticancer approach; in vitro and in vivo evidence. *Clin Exp Pharmacol Physiol* **44**, 235–243 (2017)

42. Del Rio, D., Stewart, A. J. & Pellegrini, N. A review of recent studies on malondialdehyde as toxic molecule and biological marker of oxidative stress. *Nutr Metab Cardiovasc Dis* **15**, 316–328 (2005)

43. Baltacıoğlu, E. *et al.* Lipid peroxidation levels and total oxidant/antioxidant status in serum and saliva from patients with chronic and aggressive periodontitis. Oxidative stress index: a new biomarker for periodontal disease? *J Periodontol* **85**, 1432–1441 (2014)

44. Ghallab, N. A., Hamdy, E. & Shaker, O. G. Malondialdehyde, superoxide dismutase and melatonin levels in gingival crevicular fluid of aggressive and chronic periodontitis patients. *Aust Dent J* **61**, 53–61 (2016)

45. Alizadeh, M. & Kheirouri, S. Curcumin reduces malondialdehyde and improves antioxidants in humans with diseased conditions: a comprehensive meta-analysis of randomized controlled trials. *Biomedicine (Taipei)* **9**, 23

46. Zhang, Q., Yang, J. & Wang, J. Modulatory effect of luteolin on redox homeostasis and inflammatory cytokines in a mouse model of liver cancer. *Oncology Letters* **12**, 4767–4772 (2016)

47. Khan, R. A., Khan, M. R., Sahreen, S. & Alkreathy, H. M. Effect of Launaea procumbens extract on oxidative marker, p53, and CYP 2E1: a randomized control study. *Food Nutr Res* **60**, 10.3402/fnr.v60.29790 (2016)

48. Thanh, T. B. *et al.* Protective effect of Tetracera scandens L. leaf extract against CCl4-induced acute liver injury in rats. *Asian Pacific Journal of Tropical Biomedicine* **5**, 221–227 (2015)

49. Ibrahim, Z. S., Nassan, M. A. & Soliman, M. M. Ameliorative effects of pomegranate on carbon tetrachloride hepatotoxicity in rats: A molecular and histopathological study. *Mol Med Rep* **13**, 3653–3660 (2016)

50. Hussein, R. H. & Khalifa, F. K. The protective role of ellagitannins flavonoids pretreatment against N-nitrosodiethylamine induced-hepatocellular carcinoma. *Saudi J Biol Sci* **21**, 589–596 (2014)

51. Kadasa, N. M., Abdallah, H., Afifi, M. & Gowayed, S. Hepatoprotective effects of curcumin against diethyl nitrosamine induced hepatotoxicity in albino rats. *Asian Pac J Cancer Prev* **16**, 103–108 (2015)